PHD SYNOPSIS

Name of the candidate: Anirudh S. Chellappa

Name of the Department: Department of Psychiatry

Date of registration: 01-12-2018

Title of Thesis: Constraint-Based Modeling Of Astrocyte Metabolism In Neuropsychiatric Disorders.

Guide	Biju Viswanath, Additional Professor (Psychiatry), NIMHANS	(insert signature)
Joint guide	Sanjeev Jain, Emeritus Professor (Psychiatry), NIMHANS	(insert signature)
Joint guide	Swagatika Sahoo, INSPIRE Faculty (Chemical Engineering), IIT-Madras	(insert signature)
Head of Department	Y.C. Janardhan Reddy, Professor (Psychiatry), NIMHANS	(insert signature)
Dean of Faculty	Prabha Chandra, Professor (Psychiatry), Dean (Behavioral Sciences), NIMHANS	(insert signature)

TABLE OF CONTENTS

1. Introduction....4
2. Aim & Objectives....8
2.1. Deriving the human astrocyte metabolic models....8
2.2. Using the models to identify disrupted fluxes in BD (Li+ Responders and Non-Responders) and SCZ patients' astrocytes....8
2.3. Using the models to identify the impact of loss-of-function (LoF) mutations implicated in neuropsychiatric disorders....8
3. Material and methods....10
3.1. Dataset overview....10
3.2. Pre-processing and quality control of public data....10
3.2.1. RNA-sequencing....10
3.2.2. Proteomics....11
3.3. Metabolic modeling of astrocytes....11
3.3.1. Integration of phenotype-specific astrocyte transcriptomes with Recon3D....11
3.3.2. Manual curation of astrocytic reactions for the expansion of draft metabolic models and defining model function tests....13
3.3.3. Imposing astrocytic nutrient uptake constraints....13
3.4. Identifying disrupted reactions & subSystems in BD and SCZ astrocyte metabolic models....14
3.4.1. Flux balance analysis (FBA)....14
3.4.2. Metabolic transformation algorithm (MTA)....14
3.4.3. Filtering reactions relevant to phenotype-of-interest....15
3.4.4. Metabolic subSystem enrichment analysis (MSEA)....15
3.4.5. Identifying disruptions that are significant across modules....16
3.5. Capturing the impact of loss-of-function (LoF) mutations, implicated in neuropsychiatric disorders, on astrocytes....16
3.6. Data, figures and code availability....17
4. Results and Discussion....18
4.1. Deriving and testing the human astrocyte metabolic models. (Figure.2)....18
4.2. Metabolic subsystems disrupted in BD/SCZ patients' astrocytes (Figure.3)....19
4.2.1. Slower PI-cycle in Li+ Non-Responder astrocytes. (Figure.3)....20
4.2.2. Other pathways disrupted in Li+ Non-Responder astrocytes (Figure.3)....23
4.2.3. Identifying links between PI-cycle and other disrupted lipid pathways in Li+ Non-Responder astrocytes. (Figure.4)....23
4.3. Metabolic effects of LoF mutations in SMI, AD and PD. (Figure.5-6 and Table.2)....24
5. Limitations of this study....31
6. Summary....32
7. References....33

Constraint-Based Modeling Of Astrocyte Metabolism In Neuropsychiatric Disorders.

1. Introduction.

Psychiatric disorders are a group of mental health conditions characterized by persistent changes in behavior, thoughts, moods, and emotions that can have a profound impact on an individual's daily life. These disorders could be classified into different categories, including mood disorders (e.g., depression, bipolar disorder), anxiety disorders (e.g., generalized anxiety disorder, panic disorder), impulse control disorders (e.g., attention-deficit/hyperactivity disorder), substance use disorders (alcohol and drug abuse with or without dependence), and psychotic disorders (e.g., schizophrenia). The median lifetime prevalence estimates for mood disorders are 3.3-21.4%, for anxiety disorders are 4.8-31.0%, for impulse control disorders are 0.3-25.0%, for substance use disorders are 1.3-15.0%, and for psychotic disorders are 3.06-3.48%, as estimated by epidemiology studies[1,2].

Bipolar disorder (BD) is a severe psychiatric illness characterized by manic/depressive episodes and persistent neurocognitive impairments[3], affecting 0.5% of the population (ca. 7 million in India)[4]. It is a significant cause of disability, morbidity, and mortality (15% die by suicide)[5]. Both twin and adoption studies indicate that genetics play an important role in BD, with heritability estimates ranging from 0.59 to 0.87 in twin studies[6–8]. Family/genetic strategies have also been used in efforts to validate potential subtypes of BD. The results of most such studies have been mixed, but supporting evidence is available for early versus late age at onset[9], lithium responsivity[10], psychotic BD[11], puerperal mania[12], comorbidity with panic disorder[13], a preponderantly depressed vs. preponderantly manic course[14] and unipolar mania versus typical BD[15]. A large literature has examined the relationship between BD-I and BD-II disorder, requiring, respectively, full manic versus hypomanic episodes. Recent genetic studies have shown that BD-I has a higher SNP heritability and a higher genetic correlation with schizophrenia, while BD-II has a much higher genetic correlation with MDD[16]. Advances in genotyping technology have made it possible to assay common variants in large-scale case-control studies, known as genome-wide association studies (GWAS). To date, there have been numerous GWAS studies performed on BD[17–20], with the largest and most recent conducted by the Psychiatric Genomics Consortium (PGC) reporting 64 genetic loci linked to BD through analysis of 41,917 BD patients and 371,549 controls[21]. The genes identified include those involved in ion channels, neurotransmitter transporters, and synaptic components. On the other hand, the Bipolar Sequencing Consortium (BSC), despite having a sample of 13,933 cases and 14,422 controls, had not found significant associations with any specific gene but showed promising aggregate results: novel singleton protein truncating variants in genes intolerant to loss-of-function mutations are enriched in BP patients[22].

The polygenicity of psychiatric disorders - like most complex human traits - is an unsolved scientific puzzle. The genetic architectures of complex brain diseases and disorders are closely linked to the genes whose expression defines specific brain cell-types[23]. The largest and most recent BD GWAS hits (n=64) were enriched in excitatory and inhibitory neurons over other cell types within cortical and subcortical brain regions in mice. In human brain samples, signal enrichment was also observed in hippocampal pyramidal neurons and prefrontal cortex and hippocampal interneurons compared to other cell types[21]. These findings are similar to those reported in GWAS data of schizophrenia (SCZ)[24] and major depressive disorder[25].

Clinically, BD is characterized by mood swings with the patient alternating between mania and depression[3]. Managing BD effectively requires controlling these mood episodes and preventing relapse. Mood stabilizing agents are used for this purpose, with lithium (Li+) being the first-line mood stabilizer. Li+ has been used since 1949[26], and is the only effective drug for preventing suicides[27,28] and improving cognition[29] in BD patients. While Li+ can be highly effective, not all patients respond to it: approximately 30% of patients have an excellent response, 30% show a partial response, and 40% are resistant to treatment and are considered non-responders, making their clinical management difficult[30]. When treating a chronic illness, being able to predict a patient's response to treatment is crucial for effective management. Without this capability, treatment often involves trial and error, leading to uncontrolled disease and a negative impact on long-term prognosis. The selection of mood stabilizers for BD is similarly challenging. Several studies have tried to link clinical parameters to response to Li+ treatment, but the predictive power of these remains limited[31]. To be able to predict a patient's response to Li+ would greatly benefit clinical management.

The reason for the inability to predict responses to Li+ is due to a lack of understanding of its mechanism of action. It is believed that Li+ affects brain cells by altering ongoing molecular processes, leading to changes in cellular function. The mechanism of action of Li+ in the brain is thought to be highly complex, inducing a multitude of effects on the protein expression, neurotransmission, circadian biology, ion transport, etc[32]. Two main proteins, inositol monophosphatase (IMPA1)[33] and glycogen synthase kinase-3 (GSK3)[34], have been proposed as candidate targets, with others also being considered. Both of these proteins are inhibited at Li+ concentrations that approximate therapeutic blood levels, which are 0.5-1 mEq/L[35]. The ‘inositol depletion’ hypothesis, proposed by Berridge *et al.*[36], suggests that Li+'s effectiveness in treating BD depends on inhibiting IMPA1, reducing inositol supply for phosphatidylinositol (PI) synthesis. Li+'s inhibition of IMPA1 shows unusual uncompetitive kinetics, and is seen only when the IMPA1 substrate inositol 1-phosphate (IP1) accumulates in cells. This mechanism implies selective inhibition in cells like neurons

with high PI turnover. While a knockout of IMPA1 in mice suggested altered inositol signaling[37], a suitable mouse model for BD remains elusive. GSK3 inhibition, instead of IMPA1, has been emphasized by researchers over the years[38], but GSK3 inhibitors haven't progressed to BD clinical trials. Notably, amphibian studies indicated that Li+'s effects could be blocked by inositol supplementation[39]. Observations in yeast[40] and mammalian neurons[41] demonstrated that GSK3 positively regulates myo-inositol 1-phosphate synthase, a key enzyme in inositol's de novo synthesis, further suggesting inositol homeostasis plays a vital role in Li+'s action. Inositol and GSK3 have been the main focus in understanding Li+'s mechanisms of action, emphasizing the pressing need for systematic and unbiased investigations to explore additional pathways involved.

Increasingly, it's being known that Li+ might have an influence on glial cells, especially astrocytes[42,43]. Astrocyte dysfunction has been implicated in BD[44,45] and also in the mechanism of action of Li+[42,46]. Stable isotope-resolved metabolomics (SIRM) approach showed that Li+ enhanced glycolytic and Krebs cycle activity in both astrocytes and neurons, especially the anaplerotic pyruvate carboxylation (PC). The study also showed that Li+ stimulated the extracellular release of 13C labeled -lactate, -alanine (Ala), -citrate, and -glutamine (Gln), specifically by astrocytes[42]. It has also been shown that concentration of myo-inositol is higher in astrocytes than in neurons, and has been widely considered an astroglial metabolic marker[47]. In addition, cortical neuron cultures do not express the enzyme myo-inositol phosphate synthase (MIP-synthase), but rather depend on extracellular supply of myo-inositol[48]. Overall, these observations make astrocytes more attractive and a probable candidate for Li+'s action leading to myo-inositol homeostasis in the brain, compared to neurons.

Because screening for these metabolic pathways in astrocytes, in-vivo or in-vitro, is a substantial task, we adopted an alternative, computational approach to narrow down towards putative candidates that could be experimentally validated. First, by integrating publicly-available transcriptomics and proteomics data with the constraint-based reconstruction and analysis (COBRA) framework[49], we have derived genome-scale metabolic models (GSMM) of astrocytes derived from BD, SCZ patients and healthy controls. We improved upon prior brain metabolic models by extensive manual curation of literature to identify the metabolic functions and extracellular nutrient uptake constraints relevant to astrocytes. In BD, we derived separate metabolic models for Li+ responders and non-responders to analyze metabolic fluxes related to treatment responsiveness. Despite the shared clinical symptomatology, genetics and biology between BD and SCZ, there is limited evidence supporting the effectiveness of Li+ as a standalone treatment for SCZ patients[50]. To explore the specificity of Li+'s efficacy in BD compared to SCZ, we hypothesized that it might be reflected at the molecular/metabolic level, and thus we derived metabolic models of astrocytes from SCZ patients, particularly monozygotic twin

pairs (SCZ twins and Healthy twins), along with matched controls. And subsequently, by using diverse analytical methods we have identified metabolic fluxes that are specifically disrupted in the astrocytes of BD, BD-Responders, BD-NonResponders and SCZ Twins, as compared to healthy/control models, thereby gaining insights into the differences between these conditions.

One of the advantages of GSMM is that it can describe the metabolic state of cells at a steady state without the need for detailed knowledge of enzymatic kinetics[49], which is difficult to estimate at a network level. Modeling studies like this have been extensively used in the past decade to explain not only human metabolism in general[51] but also the effects of human disease phenotypes[52–55].

2. Aim & Objectives.

To generate genome-scale metabolic models of human astrocytes using publicly available 'omic data obtained from psychiatrically ill patients and healthy controls, and explore the metabolic changes associated with treatment responsiveness to Li+ in BD, but also to understand the shared metabolic biology with other psychiatric disorders like SCZ (Figure.1).

The objectives were as follows:

2.1. Deriving the human astrocyte metabolic models.

a. Pre-processing and quality control of public data.
b. Integrating phenotype-specific transcriptomes and glial proteome data with Recon3D.
c. Expanding draft models through manual curation of literature.
d. Imposing experimental nutrient uptake constraints.

2.2. Using the models to identify disrupted fluxes in BD (Li+ Responders and Non-Responders) and SCZ patients' astrocytes.

a. Setting up the analytical methods to solve metabolic models.
b. Filtering reactions relevant to phenotype-of-interest.
c. Metabolic-subSystem enrichment analysis (MSEA).
d. Identifying disruptions that are significant across modules.

2.3. Using the models to identify the impact of loss-of-function (LoF) mutations implicated in neuropsychiatric disorders.

a. Curating the genes with LoF mutations implicated in severe mental illness (SMI), Alzheimer's disease (AD) and Parkinson's disease (PD).
b. Setting up the analytical method to simulate the effects of LoF mutations on the metabolic models.
c. Identifying the fluxes disrupted by LoF mutations.

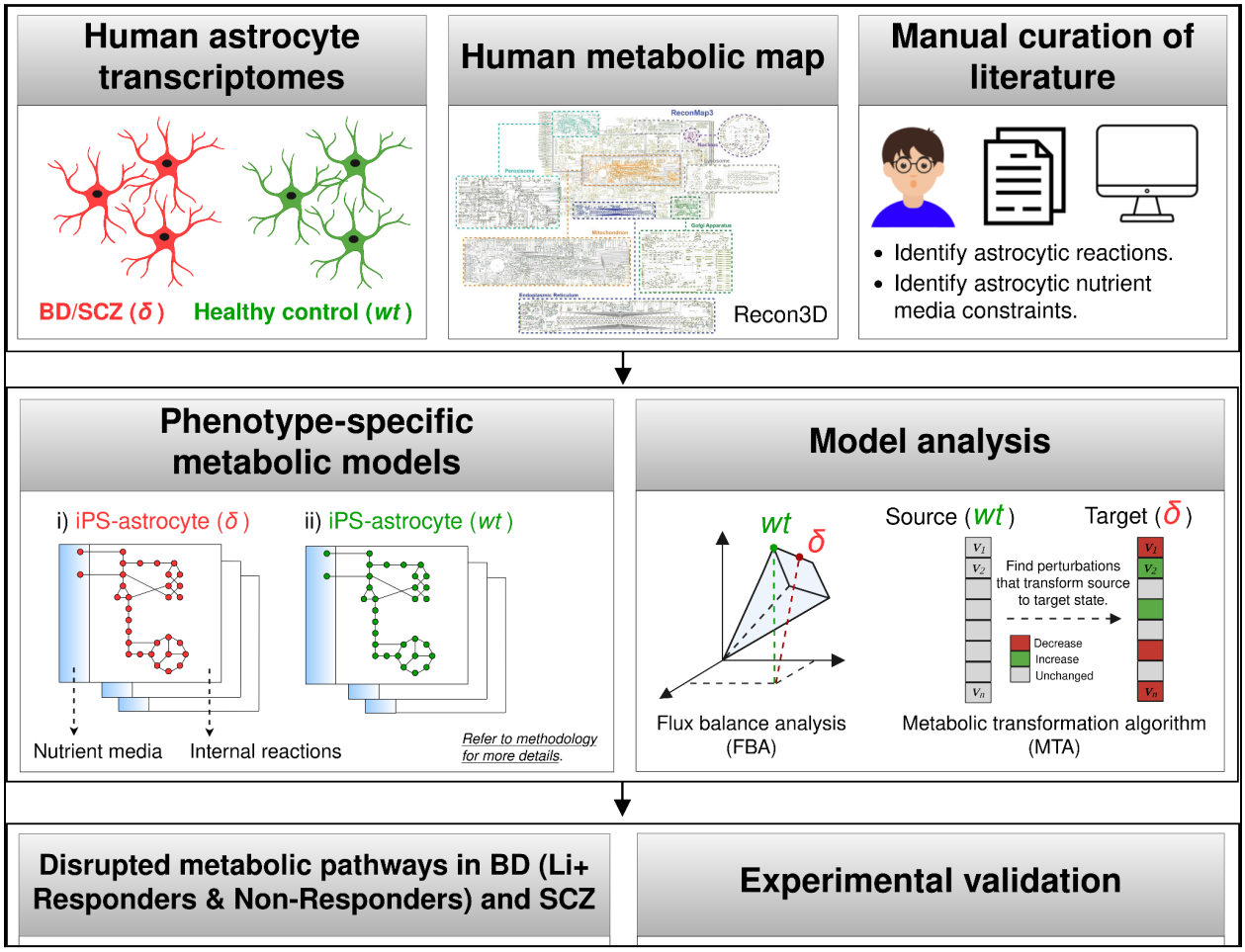

Figure.1. Graphical abstract. Constraint-Based Modeling Of Astrocyte Metabolism In Neuropsychiatric Disorders. Firstly, genome-scale metabolic models (GSMM) of astrocytes from BD, SCZ patients, and healthy controls were constructed by integrating publicly-available transcriptomics data, proteomics data with the constraint-based reconstruction and analysis (COBRA) framework. Separate metabolic models for Li+ responders and non-responders were derived to analyze metabolic fluxes related to treatment responsiveness. Metabolic models of astrocytes from SCZ patients were derived to explore the shared metabolic phenotypes with BD. Enhancements to previous brain metabolic models were achieved through comprehensive manual curation of literature, identifying relevant metabolic functions and extracellular nutrient uptake constraints relevant to astrocytes. Subsequently, diverse analytical methods were employed to identify disrupted metabolic fluxes in astrocytes from BD, BD-Responders, BD-NonResponders and SCZ Twins.

3. Material and methods.

3.1. Dataset overview

Three previously published transcriptome datasets: "Zhang"[56], "Vadodaria"[45], “Koskuvi”[57], were utilized. In Zhang, the astrocytes were purified from mice, human fetal, and adult brain tissues using immunopanning. The mice data were excluded from our analysis leaving us with 41 human subjects including six fetal astrocyte samples, 12 adult astrocyte samples, eight glioblastoma multiforme (GBM) or sclerotic hippocampal samples, four whole human cortex samples, and 11 human samples of other purified CNS cell types. Healthy astrocytes, except for the GBM and sclerotic samples, were obtained from fetal brain tissue from elective pregnancy terminations at 17–20 gestational weeks or healthy temporal lobe cortices from patients undergoing neurological surgeries. In Vadodaria, the astrocytes were derived from induced pluripotent stem (iPS) cells generated from fibroblasts of BD patients (n=5), which includes both Li+ responders (n=3) and non-responders (n=2), as well as healthy controls (n=4). The astrocytes were differentiated for five weeks, and subsequently stimulated with 10 ng/mL IL-1b or phosphate buffered saline (PBS) for 5h, followed by RNA-Seq. Similarly, in Koskuvi, the astrocytes were derived from iPS cells generated from fibroblasts of monozygotic twin pairs discordant for SCZ (n=4), which includes both healthy twins (HT, n=4) and SCZ twins (ST, n=4), as well as age- and sex- matched healthy controls (n=6). RNA was extracted from the monolayer culture of iPS-derived astrocytes (150 DIV i.e., days in vitro), followed by RNA-Seq. All three datasets were uniformly processed using a consensus set of tools. After processing and quality control, "Zhang" was used to derive metabolic models of primary astrocytes, while "Vadodaria" and “Koskuvi” were used to derive metabolic models of iPS-astrocytes.

3.2. Pre-processing and quality control of public data

3.2.1. RNA-sequencing

Transcriptome data (FastQ) were obtained by downloading from public repositories (Zhang/Vadodaria/Koskuvi). The non-human samples, if any, were removed from Zhang, Vadodaria and Koskuvi. FastQC (http://www.bioinformatics.babraham.ac.uk/projects/fastqc) was used to assess the quality of the reads and Cutadapt (https://cutadapt.readthedocs.io/en/stable/) was used to remove adapter contamination. HISAT2[58] was used to align the filtered reads to the human reference genome (GRCh37). Samtools[59] was used for SAM to BAM conversion and sorting. Cufflinks[60] was used to estimate gene-level expression (FPKM), and gene symbols were annotated for NCBI Entrez IDs using org.Hs.eg.db. The non-specific genes i.e., same gene symbol mapping to multiple Entrez IDs or multiple symbols mapping to the same ID were excluded. For Zhang, Vadodaria and Koskuvi, the genes with FPKM $\geq$ 0.1 in at least

50% of all samples were considered, resulting in 13,423, 14,543 and 16,724 genes respectively.

3.2.2. Proteomics

The human cortical glial proteomics data from the human protein atlas (HPA)[61] were utilized to provide further evidence of expression in Zhang, Vadodaria and Koskuvi. The reliability scores ('Enhanced', 'Supported', 'Approved', or 'Uncertain') and the semi-quantitative nature of the immunohistochemistry protein abundance ('High', 'Medium', 'Low') were retained[62].

3.3. Metabolic modeling of astrocytes

3.3.1. Integration of phenotype-specific astrocyte transcriptomes with Recon3D

Recon3D[51], the latest human metabolic reaction library, was used to extract draft metabolic models. While all the samples in the Zhang, Vadodaria, and Koskuvi datasets were processed (FASTQ to FPKM), only a subset of samples was chosen from each dataset for metabolic modeling. In Zhang, only cortical astrocytes from adult samples (n=12) were included. In the Vadodaria dataset, only PBS treated iPS-astrocytes from BD patients (n=5) and healthy controls (n=4) were considered. However, in the Koskuvi dataset, the entire dataset, including iPS-astrocytes from SCZ twin pairs (n=4) and healthy controls (n=6), was utilized for modeling. In Vadodaria, the BD patient data was further divided into Li+ responders (n=3) and non-responders (n=2) for modeling treatment responsiveness. In Koskuvi, the monozygotic twin pairs were further divided into SCZ twins (n=4) and healthy twins (n=4) for modeling the effects of familial/genetic risk. Genes that were detected in the transcriptome (n=13,423, Zhang; n=14,543, Vadodaria; n=16,724, Koskuvi) but had ‘uncertain’ reliability in the HPA glial proteome were excluded, resulting in a subset of genes that were "transcriptome & proteome" evident (n=4,105, Zhang; n=4,040, Vadodaria; n=4,203, Koskuvi). Metabolic models for eight distinct phenotypes were obtained by constraining Recon3D with the transcriptome data of:

1. Zhang: Primary astrocytes (Primary-Ctrl),
2. Vadodaria: iPS-astrocytes from healthy controls (iPS-Ctrl-i),
3. Vadodaria: iPS-astrocytes from BD patients (iPS-BD),
4. Vadodaria: iPS-astrocytes from BD patients - responders (iPS-BD-R),
5. Vadodaria: iPS-astrocytes from BD patients - non-responders (iPS-BD-NR),
6. Koskuvi: iPS-astrocytes from healthy controls (iPS-Ctrl-ii),
7. Koskuvi: iPS-astrocytes from monozygotic twin pairs - SCZ twins (iPS-ST),
8. Koskuvi: iPS-astrocytes from monozygotic twin pairs - Healthy twins (iPS-HT).

The genes were mapped to reactions using the function *mapExpressionToReactions* in COBRA Toolbox. The reactions were associated with a core reaction set (n=1843, Zhang; n=1765, Vadodaria; n=1836, Koskuvi). Different variants of the model extraction methods (MEMs) such as iMAT[63], GIMME[64], MBA[65] and FastCore[66] were considered. Both absolute (abs) and normalized (norm) FPKM values were used to generate the metabolic models. Three gene expression thresholds ($FPKM_{abs}$, $FPKM_{norm.t1}$, $FPKM_{norm.t2}$) were used, and for each of them, the high-confidence (HC), medium-confidence (MC) and inactive (IA) reactions were defined as follows,

a.) $FPKM_{abs}$:

$$G_i = rowMax_i(abs(FPKM))$$
$$HC \leftarrow if\ G_i > 2$$
$$MC \leftarrow if\ 2 \leq G_i \geq 0.1$$
$$IA \leftarrow if\ G_i < 0.1$$

b.) $FPKM_{norm.t1}$:

$$G_i = rowMax_i(quantilenorm(log10(FPKM + 1)))$$
$$HC \leftarrow if\ G_i > 50th\ percentile(\overline{G})$$
$$MC \leftarrow if\ 50th\ percentile(\overline{G}) \leq G_i \geq 25th\ percentile(\overline{G})$$
$$IA \leftarrow if\ G_i < 25th\ percentile(\overline{G})$$

c.) $FPKM_{norm.t2}$:

$$G_i = rowMax_i(quantilenorm(log10(FPKM + 1)))$$
$$HC \leftarrow if\ G_i > 25th\ percentile(\overline{G})$$
$$MC \leftarrow if\ 25th\ percentile(\overline{G}) \leq G_i \geq 10th\ percentile(\overline{G})$$
$$IA \leftarrow if\ G_i < 10th\ percentile(\overline{G})$$

Where G_i is the maximum expression value of the i^{th} gene across all samples. The above thresholds were also used to define inactive reactions (IA), unless manual curation of literature dictated otherwise.

Draft metabolic models of astrocytes were generated from the transcriptomes of eight phenotypes (Primary-Ctrl, iPS-Ctrl-i, iPS-BD, iPS-BD-R, iPS-BD-NR, iPS-Ctrl-ii, iPS-ST and

iPS-HT) using four MEMs (iMAT, GIMME, MBA, and FastCore) across three gene expression thresholds ($FPKM_{abs}$, $FPKM_{norm.t1}$, $FPKM_{norm.t2}$). iMAT and MBA require a 'medium-confidence' threshold to be defined by users, while GIMME and FastCore do not. The MEMs maximize the number of high-confidence and minimize the number of medium-confidence reactions in their output models. The 24 models that captured the least fluxInconsistent reactions, the highest number of core reactions, and the highest overlap with astrocytic reactions (n=649) from Lewis et al. 2010, for each of the eight phenotypes, were chosen for further expansion.

3.3.2. Manual curation of astrocytic reactions for the expansion of draft metabolic models and defining model function tests

Extensive manual curation of the literature was conducted to identify biochemical reactions (n=159) in astrocytes, which exhibited behavioral, cellular, or molecular phenotypes upon disruption. Their rationale for inclusion, along with PMIDs supporting and refuting their activity in astrocytes, was also provided. Most of the literature evidence was derived from studies on rodent models. While these curated reactions were mostly part of Recon3D, a significant number of them were not detected by the automated model extraction methods (MEMs) across all 24 models. Consequently, it became necessary to identify the missing metabolites and reactions, conduct gap-filling, and incorporate these reactions into the models. As part of this effort, an additional extracellular compartment 'synapse' [s], along with exchange (n=15) and transport reactions (n=14), were included in the 'Primary-Ctrl' models to capture astrocyte-synapse metabolic crosstalk. However, the synaptic compartment and corresponding reactions were not included in the iPS-astrocyte models. Additionally, the curated reactions were also used as model function tests (MFTs), ensuring that all 24 models carried non-zero flux through the curated reactions, subject to nutrient media constraints.

3.3.3. Imposing astrocytic nutrient uptake constraints

It was assumed that in vivo, all the constituents of ASM would cross the BBB and be available for uptake by astrocytes. Hence, the 'Primary-Ctrl' model's extracellular compartment [e] was constrained by all metabolites and ions that i) constitute the astrocyte sustenance medium (ASM)[67], and ii) cross the blood brain barrier (BBB)[68]. The remaining four iPS-astrocyte models' extracellular [e] compartments were constrained by ASM alone, representing culture media conditions. The metabolic components of the ASM, which consists of Neurobasal medium, Minimum Essential Medium - Non-Essential Amino Acids Solution, GlutaMAX Supplement, and N-2 Supplement, were obtained from the Thermo Fisher Scientific™ website. The metabolic components of the BBB were obtained from Thiele et al.[68]. There are 22 components that overlap between the ASM (n=44) and BBB (n=45). To simulate nutrient uptake, all nutrient uptakes in the model except for the 67

exchanges added to the extracellular compartment [e], for which uptake rates were set to -10mmol/gDw/h, were set to 0.

3.4. Identifying disrupted reactions & subSystems in BD and SCZ astrocyte metabolic models.

3.4.1. Flux balance analysis (FBA)

A metabolic network consisting of m metabolites and n reactions is represented by a stoichiometric matrix S where S_{ij} represents the stoichiometric coefficient of metabolite i in reaction j. The flux vector for each reaction in the network is represented by v. Flux balance analysis (FBA) assumes a steady-state mass balance wherein the sum of the input flux equals the sum of the output flux. This follows as, $dx_i / dt = 0$ i.e. the change in concentration of the i^{th} metabolite over time is zero[69]. Flux variability analysis (FVA) was used to calculate the minimum and maximum flux through each reaction in all five metabolic models subject to constraints,

$$min/max\ c^t\ x,\ s.t.\quad s.v = dx/dt = 0\,, \tag{1}$$

$$v_{min} \le v_j \le v_{max}\,, \tag{2}$$

where the equation (1) corresponds to the steady-state mass-balance constraints, whereas equation (2) corresponds to the reaction directionality and capacity constraints. The ratio of flux span (FSr)[70] for each reaction was calculated as follows,

$$FSr\ (healthy\ vs\ disease) = \frac{abs(FVAmax_{j,healthy} - FVAmin_{j,healthy})}{abs(FVAmax_{j,disease} - FVAmin_{j,disease})}\,, \tag{3}$$

where $FVAmax$ and $FVAmin$ are the maximum and minimal flux through the j^{th} reaction in the model. FSr can be calculated only for those reactions that are captured by both the models under comparison. The reactions with $FSr > 1.5\ and < 0.8$ were identified for each phenotype-of-interest (n=4 i.e., BD; BD_Responder; BD_NonResponder; SCZ-Twin), and subsequently considered for downstream analysis.

3.4.2. Metabolic transformation algorithm (MTA)

The metabolic transformation algorithm (MTA)[52,71,72] identifies reactions in a metabolic network whose inhibition facilitates a transformation between two metabolic states (e.g., from diseased to healthy states, or vice-versa). The inputs to MTA are i) the transcriptomic measurements of the source and target states, and ii) the reference metabolic model. For each transformation analysis, MTA follows a two-step process: i) determining the flux

distribution of the source metabolic state (v^{ref}) using iMAT followed by ACHR sampling of the solution space. ii) determining the set of genes whose expression has significantly elevated or reduced between the source and target states. Using i) and ii), MTA computes a transformation score for each of the metabolic reactions in the cell, and usually, the 10-20% reactions with the highest MTA score contain promising candidate targets. For each phenotype-of-interest, we ran MTA twice, by swapping the source and the target states. E.g., in order to identify the reactions relevant to BD, we identified the reactions that transformed i) "iPS-Ctrl" to "iPS-BD", and ii) "iPS-BD" to "iPS-Ctrl". For either runs, the top 20% predictions were first identified, and subsequently their union sets were considered for downstream analysis.

3.4.3. Filtering reactions relevant to phenotype-of-interest.

From the reactions as identified by FVA ($FSr > 1.5\ and < 0.8$) or MTA (top 20%), filters were applied to select for reactions that were relevant to the phenotype-of-interest. While defining the filters, it was important to consider the fact that the treatment responders and the non-responders together comprise the BD cohort. Hence the fluxes relevant to "BD_R" and "BD_NR'' can share overlaps with "BD".

Phenotype-of-interest	**Filtering criteria**
BD[a]	Specifically disrupted in "iPS-Ctrl vs iPS-BD" & unchanged between control models.
BD-Responder[b]	Specifically disrupted in "iPS-Ctrl vs iPS-BD-Responder" & unchanged between control models.
BD-NonResponder[c]	Specifically disrupted in "iPS-Ctrl vs iPS-BD-NonResponder" & unchanged between control models.
SCZ-Twin[d]	Specifically disrupted in "iPS-Ctrl vs iPS-SCZ-Twin" & unchanged between control models.
[a]Can share overlaps with BD-Responder, BD-NonResponder and SCZ-Twin. [b]Can share overlaps with BD and SCZ-Twin but not with BD-NonResponder. [c]Can share overlaps with BD and SCZ-Twin but not with BD-Responder. [d]Can share overlaps with BD, BD-Responder and BD-NonResponder.	

Table.1. Reaction filtering criteria. "Unchanged between control models" means the reactions that were not found to be disrupted in "iPS-Ctrl vs Primary-Ctrl".

3.4.4. Metabolic subSystem enrichment analysis (MSEA).

To test for enrichment of disrupted metabolic subSystems, a hypergeometric test was applied to each subSystem, and the P-value was calculated for each subSystem using the *phyper* function in *R* (equation 4) as below,

$$phyper(x - 1,\ m,\ n - m,\ k, lower.tail = FALSE) \quad (4)$$

Where n is the number of all reactions in the model, k is the number of the disrupted reactions within each tested subSystem, m is the total number of reactions within each disrupted subSystem, and x is the overlap size between k and m. This was followed by multiple-testing corrections using the Benjamini-Hochberg false discovery rate[73], and subSystems with $P_{FDR} < 0.05$ were considered as significant.

3.4.5. Identifying disruptions that are significant across modules.

Here, a 'module' was defined as the list of subSystems that were predicted to be significant by MSEA, using either of the analytical approaches i.e., FBA/MTA. E.g. 'FVA_BD_NR_norm_t1' is a module - where 'FVA' is the analytical method, 'BD_NR' is the phenotype-of-interest and 'norm_t1' is the gene expression thresholding of the metabolic model. For each phenotype-of-interest (BD, BD-Responder, BD-NonResponder and SCZ-Twin), we generated six modules (i.e., derived using three expression thresholds and two analytical methods), and identified the subSystems that were <u>disrupted in at least two or more modules</u>.

3.5. Capturing the impact of loss-of-function (LoF) mutations, implicated in neuropsychiatric disorders, on astrocytes.

A collection of genes (n=154) implicated in various neuropsychiatric disorders (SMI, AD, and PD) was curated. This analysis was specifically restricted to the genes identified from in-house studies on SMI (n=120)[74,75] and AD (n=26)[76], as well as the genes known to impact astrocytes in PD (n=8)[77]. The cobratoolbox's *findRxnsActiveWithGenes* function was utilized to map individual genes to their corresponding reactions in the control metabolic models, namely the 'Primary-Ctrl' and 'iPS-Ctrl-i' models. Among the 154 genes, those that were not captured by Recon3D or the two control metabolic models, were excluded from this analysis. Subsequently, to simulate the LoF of a particular gene, an LoF model was created in which the upper (ub) and the lower bounds (lb) of the mapped reactions were constrained by 50% of wt model's optima, i.e.,

$$ub_{r,LoF} = max_{r,wt}/2, \quad (5)$$

$$lb_{r,LoF} = min_{r,wt}/2, \quad (6)$$

Afterward, both the *LoF* and *wt* models underwent FVA, and reactions with FSr > 1.5 and < 0.8 in the LoF condition were determined for each gene included in this analysis. The perturbation class of the disrupted reactions was annotated as 'DirectMapping' if the reaction was directly mapped by the gene, or as 'Cascade' if the reaction was captured as a

consequence of the perturbation of another 'DirectMapping' reaction. This information indicates whether the disruption was limited to the reaction directly catalyzed by the gene itself (DirectMapping) or if it led to a domino effect (Cascade).

3.6. Data, figures and code availability.

This study did not generate experimental data. Raw transcriptome data used in this study were publicly available. Figure panels were generated programmatically in R with the exception of Fig.1, Fig.3.b-c, and Fig.4 which was created using BioRender.com (full license) and Diagrams.net (open source). All original code has been deposited at GitHub and will be made publicly available.

4. Results and Discussion.

4.1. Deriving and testing the human astrocyte metabolic models. (Figure.2)

Draft metabolic models of astrocytes (n=56) were extracted for eight distinct phenotypes, including BD patients (iPS-BD, iPS-BD-R, iPS-BD-NR), SCZ twin (iPS-ST), healthy twin (iPS-HT) and healthy controls (Primary-Ctrl, iPS-Ctrl-i, iPS-Ctrl-ii), by using transcriptome data and glial proteomics data as a constraint on the Recon3D human metabolic knowledgebase. The gene expression threshold determines the model contents, and there's no one model that's poised to explain the underlying biology[78]. Hence, three metabolic models were derived for each of the eight phenotypes by using different FPKM thresholds. Of the 56 models, only the iMAT-derived models (n=24) satisfied our selection criteria and only those were further expanded (refer Methodology section 3.3. for more details). First, the properties of the 24 models, before (preExpansion) and after expansion (postExpansion), were evaluated (**Fig.2.a-e**). The final models (i.e., postExpansion) consisted of 5,342–6,305 reactions and 3,679–4,273 metabolites. The flux inconsistency, which refers to the blocked reactions, ranged between ~22-29% in the final models, which is primarily driven by the nutrient media constraints, as opposed to zero blocked reactions in the draft models due to the unconstrained nutrient media. This constraint was necessary to ensure that the final models operated solely on physiologically relevant nutrient media conditions. The core reactions captured by all models ranged between ~70-98%, and the Lewis et al. astrocytic reactions captured by all models ranged between ~40-53%. The literature curated reactions (n=159) were also used as "metabolic tasks", and all 24 models passed ~90-93% of the tasks. A comparison was performed between our models (This Study, n=24) and previously published mass-action models of brain metabolism (Predecessor, n=11) (**Fig.2.f-g**). The growth in the size of the models over time is mainly due to the ongoing development of larger metabolic knowledge bases like Recon3D. Overall, the statistics indicated that our models do recapitulate astrocyte physiology; were in-par with its equivalents[53] and were ready to be deployed for downstream analysis. We have provided the comprehensive details of all 24 models on Github for open access for the scientific community.

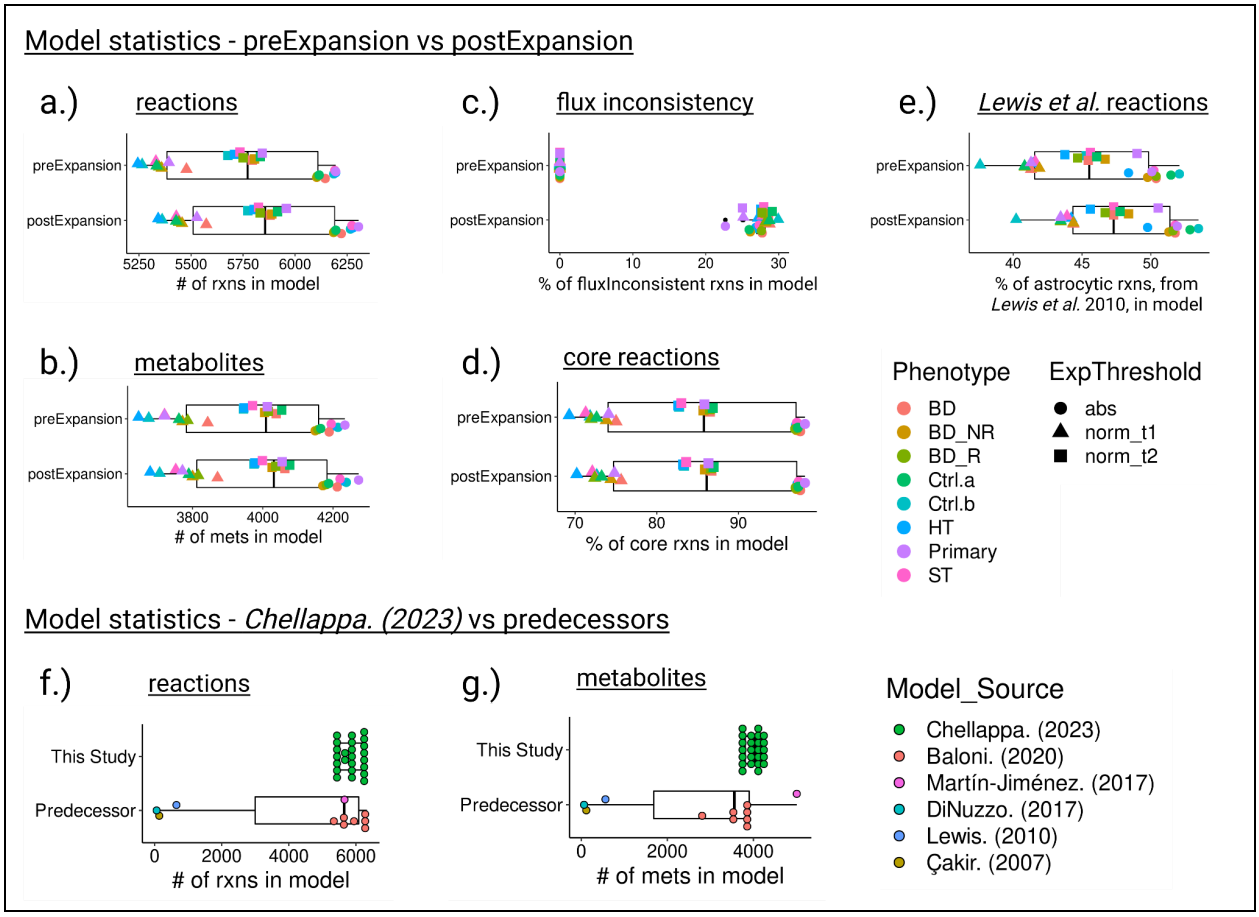

Figure.2: **Model statistics**. (a-e) Differences in model statistics observed between the iMAT-derived draft models (preExpansion, n=24) and the final models (postExpansion, n=24) of astrocyte metabolism, that were generated for five phenotypes across three gene expression thresholds. The model statistics include the # of reactions, # of metabolites, % of flux inconsistent reactions, % of core reactions and % of astrocytic reactions (Lewis et al. 2010), captured in the respective models. (f-g) Differences in model statistics observed between the models that were derived as a part of this study (This Study, n=24) and those captured by previous studies (Predecessor, n=11). Due to the unavailability of the reconstructions for most of the predecessors, with the exception of Lewis et al. (2010) and Baloni et al. (2020), only the # of reactions and metabolites were compared.

4.2. Metabolic subsystems disrupted in BD/SCZ patients' astrocytes (Figure.3)

To identify fluxes that are disrupted in our phenotypes-of-interest (BD, BD-Responder, BD-NonResponder and SCZ-Twin), the models (n=24) were first divided into groups based on their FPKM thresholds (n=3). This resulted in five models within each group. The flux distributions of the models within each group were analyzed using two methods - FVA and MTA. Filters were applied to select for reactions that were relevant to each

phenotype-of-interest, followed by Metabolic-subSystem enrichment analysis (MSEA). The metabolic subsystems that were disrupted ($P_{FDR} < 0.05$) in at least two or more modules were identified (Refer to the Methodology section 3.4. for more details). Thirteen subsystems were predicted to be disrupted by at least two or more modules across either of the four phenotypes-of-interest (**Fig.3.a**). However, none of these disruptions were found to be significant across all six modules while considering the $mean(P_{FDR}) < 0.05$.

4.2.1. Slower PI-cycle in Li+ Non-Responder astrocytes. (Figure.3)

Eight subsystems were predicted to be specifically disrupted in the Li+ non-responders models, while three subsystems were specifically disrupted in the Li+ responders models. There were no subsystems disrupted across both Li+ responders and non-responders (**Fig.3.b**). Among the eight disrupted subsystems in non-responders, inositol phosphate (IP) metabolism was captured by two modules (**Fig.3.a**). The flux through the reactions in this pathway (n=4) was reduced, indicating slower synthesis rates compared to the Li+ responder and the control models (**Fig.3.c-d**). The myo-inositol 1-phosphate phosphatase (MI1PP/IMAPase, catalyzing $IP_1 \rightarrow$Inositol), one of the four disrupted reactions in the IP metabolism, has a long-standing association with Li+'s mechanisms of action[36]. The "inositol depletion" hypothesis posits that the depletion of inositol by Li+ reduces the brain excitability in BD[36]. And this may happen through the ability of Li+ to,

1. Inhibit MI1PP activity[36],
2. Inhibit plasma membrane inositol transporters[79],
3. Regulate the rate of inositol synthesis[80].

Our models also predict slower syntheses of phosphoinositide (PI5P4K, catalyzing $PIP \rightarrow PIP_2$) and phosphoinositols (MI145PP, catalyzing $IP_3 \rightarrow IP_2$; and MI14P4P, catalyzing $IP_2 \rightarrow IP_1$), specifically in Li+ non-responder astrocytes (**Fig.3.c)**. This seems to be consistent with Sade *et al.*[37], which suggests that Li+ affects the entire phosphatidylinositol (PI) signaling system in two ways: first, by depleting inositol, thereby reducing phosphoinositide levels; and second, by elevating inositol monophosphate levels, leading to phosphoinositols accumulation.

Regardless of the molecular mechanism of Li+ action, in BD patients inositol concentrations can change, and may be further altered by Li+ treatment[81]. In contrast to the majority of metabolism studies that focus on metabolite concentrations, our model predictions are exclusively on fluxes, which represent the rates of reactions, and alterations in flux levels do not always indicate changes in metabolite concentrations[82]. Metabolite concentrations in a cell can increase due to fast synthesis or slower degradation processes. As a result, two

interpretations can be derived from our model prediction of slower rates of synthesis of inositol, PIP_2, IP_2 and IP_1, specifically in Li+ non-responders:

1. Our models challenge the depletion hypothesis, expecting a faster PI cycle (specifically a higher flux through MI1PP and PI5P4K) for its metabolites (inositol and PIP_2) to accumulate in BD patients. This implies that there may be other factors contributing to the slower PI cycle observed in Li+ non-responders.

2. Alternatively, the slower PI cycle could be indicative of lower enzyme concentrations that hinder the actions of Li+ and subsequently impact the responsiveness in BD patients. It is important to note that the slower PI cycle is only observed in the models of Li+ non-responders, while in Li+ responders, the inositol fluxes remain unaffected. This might suggest that the levels of inositol monophosphatase (IMPAse), and/or the other enzymes in the PI cycle, may be maintained at a higher level in Li+ responders, facilitating the desired response.

While the latter explanation appears to be the most plausible and parsimonious based on our predictions, experimental validation is necessary to confirm these hypotheses. Our models successfully capture the disruption of the phosphatidylinositol (PI) signaling system, a well-known aspect of Li+ biology[37,81]. This validation enhances trust in the model predictions, and justifies further investigation of the novel predictions, such as the involvement of remaining seven disrupted subsystems in Li+ non-responders that may not have been previously reported in the literature regarding BD/Li+ biology.

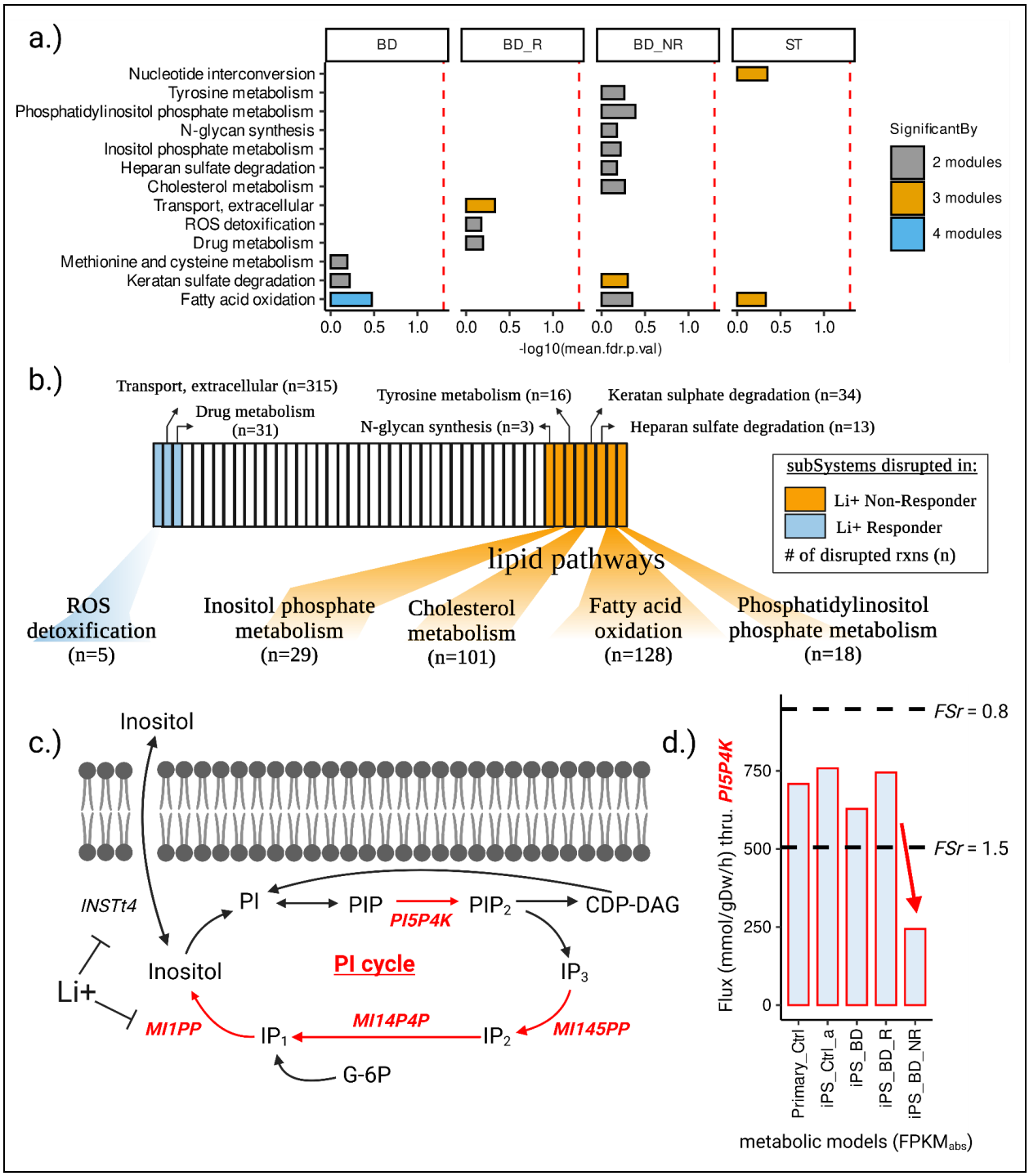

Figure.3: **Metabolic subsystems disrupted in BD and SCZ patients' astrocytes**. **(a)** Metabolic subSystems (n=13) predicted to be disrupted by at least two or more modules across either of the four phenotypes-of-interest (BD, BD-Responder, BD-NonResponder and SCZ-Twin). **(b)** Metabolic subSystems predicted to be disrupted by at least two or more modules in Li+ responders (n=3) and non-responders (n=8). The 'n' is the total # of disrupted reactions in each subSystem that could be captured by either of the six modules.

(c) Metabolic fluxes (n=4) through the inositol phosphate metabolism cycle were found to be reduced (red) specifically in Li+ non-responder metabolic models. **(d)** Bar-plot highlighting the reduction of flux through Phosphatidylinositol-5-Phosphate 4-Kinase (PI5P4K) specifically in Li+ non-responder metabolic model.

4.2.2. Other pathways disrupted in Li+ Non-Responder astrocytes (Figure.3)

Apart from inositol phosphate metabolism, the disrupted subsystems in BD-NR comprised fatty acid oxidation (FAO), cholesterol metabolism, phosphatidylinositol phosphate metabolism, tyrosine metabolism, N-glycan synthesis, keratan sulfate degradation and heparan sulfate degradation (**Fig.3.b**). However, the association of these biochemical pathways to mood/psychotic disorders remains patchy. The disruption of FAO was particularly intriguing, as it was the only one found to be perturbed across the other two phenotypes-of-interest, BD (four modules) and SCZ (three modules) (**Fig.3.a**). In all three contexts (BD, BD-NR and SCZ), disruptions in FAO were observed in both mitochondria and peroxisomes, indicating alterations in medium chain, long chain, and very-long chain fatty acids. The involvement of fatty acid oxidation (FAO) in psychotic disorders' etiology or treatment response is supported by sparse and inconsistent evidence[83]. The inconsistencies observed in these studies can be attributed to confounding factors such as medication usage, lifestyle, etc. Moreover, many of these studies investigated fatty acid alterations in peripheral samples like erythrocyte membranes, which may not necessarily corroborate findings from post-mortem brains or iPS-cells obtained from psychiatrically ill patients. However, a recent study revealed that the brain critically depends on the astrocytic oxidative phosphorylation (OxPhos) to break down fatty acids and maintain lipid balance. Disrupted astrocytic OxPhos leads to the accumulation of lipid droplets (LD) and subsequent neurodegeneration, resembling key aspects of Alzheimer's disease (AD)[84], which shares clinical symptoms and biological processes with BD and SCZ. However, the disruptions in OxPhos fluxes were not predicted by our models, likely due to degeneracy in metabolic networks[85], where a phenotype may not be apparent due to compensatory fluxes mediated through other genes/reactions.

4.2.3. Identifying links between PI-cycle and other disrupted lipid pathways in Li+ Non-Responder astrocytes. (Figure.4)

To investigate the potential coupling of PI-cycle disruptions with other seven disrupted pathways in the Li+ non-responders, the wiring diagram of pathways/fluxes feeding into and out of inositol metabolism was reconstructed (**Fig.4.**). Subsequently, the disrupted fluxes were mapped onto the wiring diagram - limited to inositol metabolism, cholesterol metabolism, and FAO, considering tractability and the close links between these three pathways. The wiring diagram revealed that fatty acids (FAs) feed into the inositol cycle through diacylglycerol (DAG), however, our models did not predict disruptions in DAG synthesis or utilization reactions. This could be attributed either to the degeneracy in

metabolic networks, or limitations of metabolic models (or mass-action models in general) to encompass other biological mechanisms that may lead to the observed metabolic phenotype. The output of FAO is acetyl-CoA, which feeds into cholesterol biosynthesis through HMG-CoA and Mevalonate. As anticipated, our models predicted disruption in the final steps of cholesterol metabolism, particularly slower fluxes through the conversion of lanosterol to cholesterol, and subsequent interconversions of cholesterol and cholesteryl esters. The disruption of brain lipid metabolism in psychoses has been inconsistent in the literature, akin to FAO, and necessitates systematic re-investigations[86]. However, the slower turnover of fatty acyl-coAs and cholesteryl esters suggests the possibility of disruptions in the biogenesis of lipid droplets (LDs), which are critical for lipid and energy homeostasis[87,88]. Accumulation of LDs has been observed in astrocytes under stress[89], and in the context of AD, astrocytes expressing the risk variant APOE4 form large LDs with impaired turnover and increased peroxidation sensitivity[90]. However, there is no literature evidence for alterations in LDs in the context of psychotic or mood disorders.

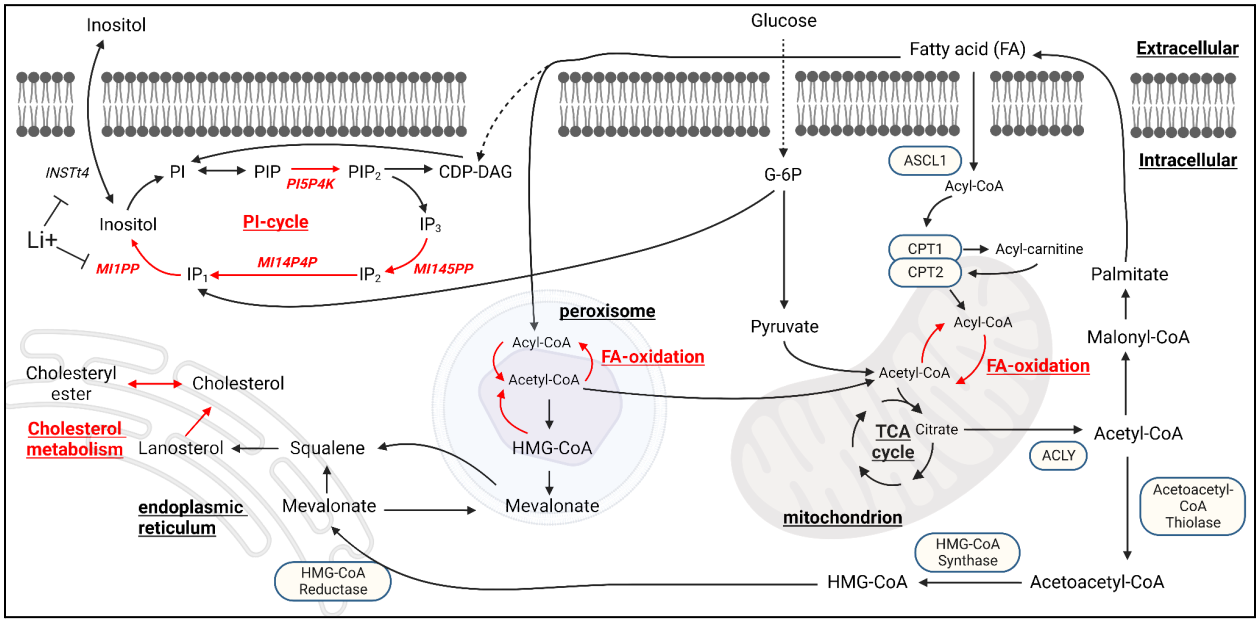

Figure.4: **Wiring diagram representing the metabolic coupling of inositol metabolism with FAO and cholesterol metabolism.** The disrupted fluxes are highlighted in red.

4.3. Metabolic effects of LoF mutations in SMI, AD and PD. (Figure.5-6 and Table.2)

Out of the 154 genes implicated in SMI, AD, and PD, only a subset (n=16) was found to be captured by the astrocyte metabolic models (Primary-Ctrl, iPS-Ctrl-i, or both) (**Fig.5.**). The attrition rate could be attributed to the fact that less than 20% of the human genome encodes metabolic reactions (biosynthesis, breakdown, or transport). For instance, only 2248 genes (as part of Recon3D) from the human genome encode metabolic reactions.

Genes captured by Recon3D but unobserved in the astrocyte metabolic models are possibly due to the gene expression threshold used for model extraction, where expression levels of the uncaptured genes fall below the threshold that was used to capture active reactions in the model. Except for *SLC29A2*, *SLC22A9* and *COASY,* the loss-of-function of the remaining 13 genes did not result in disruption of novel biochemical subsystems, i.e., subsystems other than those linked to the 'DirectMapping' reactions. However, the LoF of 12 out of the 16 genes resulted in perturbations of both 'DirectMapping' and 'Cascade' reactions in both Primary-Ctrl and iPS-Ctrl-i models. Among the remaining 4 genes, the LoF of 'GBA', 'PYGL', and 'SYNJ2' did not lead to the perturbation of 'Cascade' reactions in iPS-Ctrl, iPS-Ctrl, and Primary-Ctrl models, respectively. Additionally, the LoF of 'ASPA' did not result in the perturbation of either 'DirectMapping' or 'Cascade' reactions in both Primary-Ctrl and iPS-Ctrl-i models. The disrupted subsystems, upon the LoF of each of the 16 genes are provided in **Table.2**. Perturbation of 'DirectMapping' and 'Cascade' reactions in inositol phosphate metabolism was observed in the LoF of three genes: *INPP5A*, *SYNJ2*, and *PLCB4*. This phenotype has been well reported in the literature of Bipolar disorder and lithium biology[36], and our initial analysis of astrocyte metabolic models also captured the same in the context of BD-NonResponder. The LoF of *SLC22A9* (implicated in SMI[75]), which directly maps to mitochondrial transport reactions, was particularly interesting as its disruption led to the perturbation of cascade reactions in both FAO and fatty acid synthesis (FAS) (**Fig.6.**), a metabolic phenotype that our analytics also predicted in the context of BD, BD-NonResponder, and SCZ-Twin astrocytes.

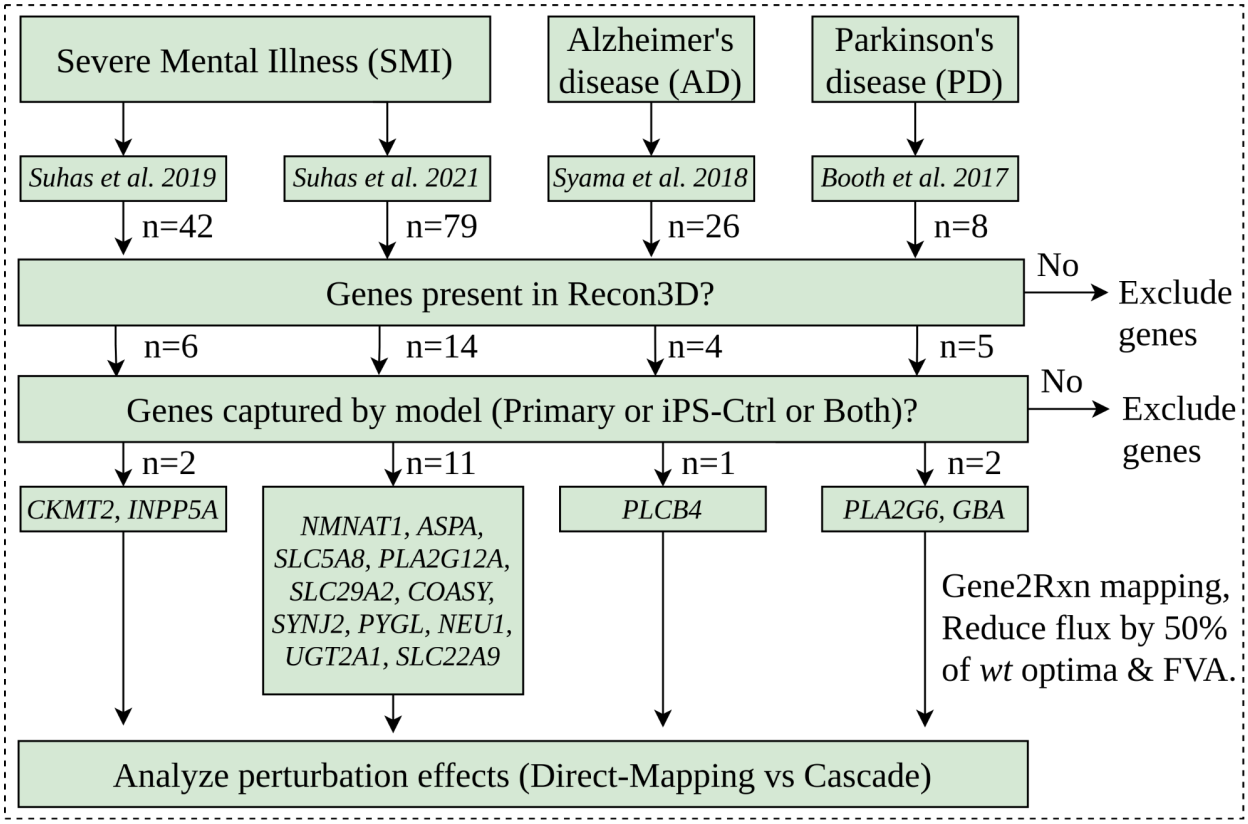

Figure.5: **Metabolic effects of LoF mutations in SMI, AD, and PD** were studied using a curated collection of genes (n=154) implicated in various neuropsychiatric disorders. The analysis focused on genes identified from in-house studies on SMI (n=120) and AD (n=26), as well as genes known to impact astrocytes in PD (n=8). Among the 154 genes, only a subset (n=16) was captured by the astrocyte metabolic models and considered for simulating LoF effects.

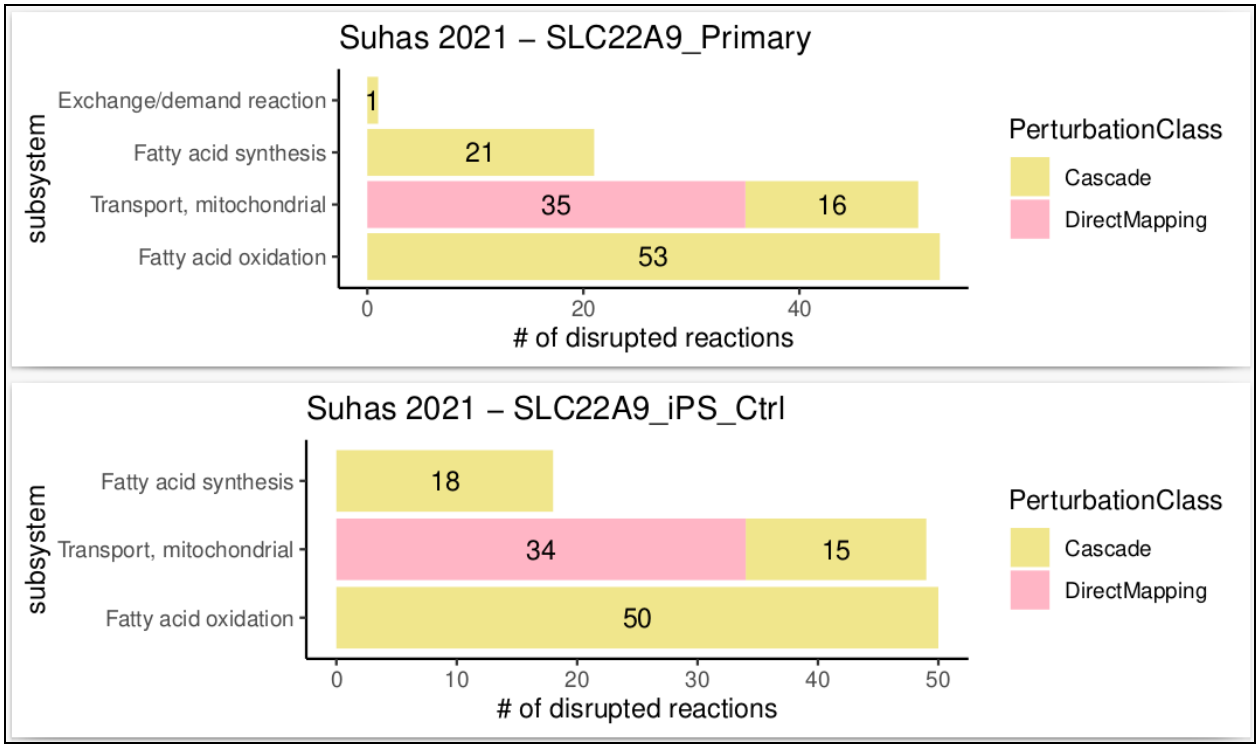

Figure.6: **The LoF of Solute Carrier Family 22 Member 9 (*SLC22A9*)** (implicated in SMI[75]), which directly maps to mitochondrial transport reactions, led to the perturbation of cascade reactions in both fatty acid synthesis (FAS) and fatty acid oxidation (FAO), in both astrocyte metabolic models (Primary-Ctrl and iPS-Ctrl).

Table.2: Metabolic subsystems disrupted upon the LoF of genes implicated in SMI, AD, PD:

	Phe no-t ype	Study	Gene Symbol	# of disrup ted rxns Prima ry-Ctrl	disrupted subsystems Primary-Ctrl	# of disrup ted rxns iPS-Ct rl-i	disrupted subsystems iPS-Ctrl-i
1.	SMI	Suhas 2019	*CKMT2*	3	Urea cycle	3	Urea cycle
2.	SMI	Suhas 2019	*INPP5A*	9	Inositol phosphate metabolism	6	Inositol phosphate metabolism
3.	SMI	Suhas 2021	NMNAT1	6	NAD metabolism Transport, nuclear	7	NAD metabolism Transport, nuclear
4.	SMI	Suhas 2021	ASPA	NIL	NIL	NIL	NIL
5.	SMI	Suhas 2021	SLC5A8	6	Transport, extracellular	6	Transport, extracellular
6.	SMI	Suhas 2021	PLA2G12 A	165	Glycerophospholi pid metabolism Exchange/deman d reaction Transport, extracellular	167	Glycerophosphol ipid metabolism Exchange/dema nd reaction Transport, extracellular
7.	SMI	Suhas 2021	SLC29A2	33	Transport, extracellular Nucleotide interconversion Transport, mitochondrial Transport, nuclear Exchange/deman	33	Transport, extracellular Nucleotide interconversion Transport, mitochondrial Transport, nuclear Exchange/dema

					d reaction Purine catabolism		nd reaction
8.	SMI	Suhas 2021	COASY	7	CoA synthesis CoA catabolism Transport, mitochondrial	7	CoA synthesis CoA catabolism Transport, mitochondrial
9.	SMI	Suhas 2021	SYNJ2	5	Inositol phosphate metabolism	2	Inositol phosphate metabolism
10.	SMI	Suhas 2021	PYGL	5	Starch and sucrose metabolism	2	Starch and sucrose metabolism
11.	SMI	Suhas 2021	NEU1	NIL	NIL	NIL	NIL
12.	SMI	Suhas 2021	UGT2A1	NIL	NIL	NIL	NIL
13.	SMI	Suhas 2021	SLC22A9	126	Fatty acid oxidation Fatty acid synthesis Transport, mitochondrial Exchange/demand reaction	117	Fatty acid oxidation Fatty acid synthesis Transport, mitochondrial
14.	AD	Syama 2018	PLCB4	4	Inositol phosphate metabolism	4	Inositol phosphate metabolism
15.	PD	Booth 2017	PLA2G6	164	Glycerophospholipid metabolism Exchange/demand reaction Transport, extracellular	167	Glycerophospholipid metabolism Exchange/demand reaction Transport, extracellular

16.	PD	Booth 2017	GBA	1	Sphingolipid metabolism	4	Sphingolipid metabolism Transport, lysosomal

5. Limitations of this study.

1. Experimental data was not directly used for deriving the models. Instead, I utilized astrocyte RNA-Seq and glial proteomics data as constraints, but their correlation with metabolite levels and fluxes is weak. Ideally, incorporating metabolomics, physiological nutrient uptake rates, and astrocyte metabolic dry-weight in BD/SCZ/Ctrl would be essential for a more comprehensive analysis of metabolic flux.
2. I did not account for neuron-astrocyte interactions, particularly the impact of astrocyte metabolism on neuronal firing and ion channel movements (e.g., Na+/K+ ions).
3. Regulatory constraints such as allosteric feedback were not considered in the model.
4. Statistical analysis directly on flux values was challenging due to the uniqueness of objective values. Repeating the simulation with the same constraints yielded identical results through the objective function.

6. Summary.

Computational models of astrocyte metabolism were constructed and utilized to analyze metabolic fluxes in BD and SCZ, as well as to examine the effects of LoF mutations in genes associated with neuropsychiatric disorders like SMI, AD, and PD. Through this process of deriving and analyzing patients' astrocyte metabolic models, four mutually exclusive hypotheses were formulated for further experimental validation:

1. Slower fatty acid oxidation rates were observed in BD, BD-NonResponders, and SCZ-Twin astrocytes. To test this, levels of acylcarnitine or carnitine palmitoyltransferase I (CPT1), a rate-limiting step in fatty acid oxidation, can be measured in both BD and SCZ patients' astrocytes since this pathway was disrupted in both phenotypes.

2. Slower cholesterol synthesis and inositol metabolism were specifically observed in BD-NonResponders. This can be investigated using untargeted lipidomics of BD patients' astrocytes.

3. Slower turnover of fatty acyl-coAs and cholesteryl esters, in BD-NonResponders, suggests the possibility of disruptions in the biogenesis/expansion of lipid droplets (LDs). This can be investigated by analyzing/profiling LDs[91], in BD patients' astrocytes.

4. Maintaining the astrocytic inositol synthesis rate (i.e., faster PI cycle) was identified as a necessary condition for Li+ responsiveness in BD. This can only be tested through stable-isotope tracing experiments, probing inositol metabolism using 13C-labeled myo-inositol[92], in BD patients' astrocytes.

The experimental validation of the above hypotheses has been initiated.

7. References.

1. KESSLER, R. C. *et al.* Lifetime prevalence and age-of-onset distributions of mental disorders in the World Health Organization's World Mental Health Survey Initiative. *World Psychiatry* **6**, 168–176 (2007).
2. Perälä, J. *et al.* Lifetime prevalence of psychotic and bipolar I disorders in a general population. *Arch. Gen. Psychiatry* **64**, 19–28 (2007).
3. Grande, I., Berk, M., Birmaher, B. & Vieta, E. Bipolar disorder. *The Lancet* **387**, 1561–1572 (2016).
4. Murray, C. J. L. & Lopez, A. D. Measuring global health: motivation and evolution of the Global Burden of Disease Study. *The Lancet* **390**, 1460–1464 (2017).
5. Miller, J. N. & Black, D. W. Bipolar Disorder and Suicide: a Review. *Curr. Psychiatry Rep.* **22**, 6 (2020).
6. Smoller, J. W. & Finn, C. T. Family, twin, and adoption studies of bipolar disorder. *Am. J. Med. Genet. C Semin. Med. Genet.* **123C**, 48–58 (2003).
7. Mendlewicz, J. & Rainer, J. D. Adoption study supporting genetic transmission in manic--depressive illness. *Nature* **268**, 327–329 (1977).
8. Kendler, K. S., Ohlsson, H., Sundquist, J. & Sundquist, K. An Extended Swedish National Adoption Study of Bipolar Disorder Illness and Cross-Generational Familial Association With Schizophrenia and Major Depression. *JAMA Psychiatry* **77**, 814 (2020).
9. Schürhoff, F. *et al.* Early and late onset bipolar disorders: two different forms of manic-depressive illness? *J. Affect. Disord.* **58**, 215–221 (2000).
10. Alda, M., Grof, P., Grof, E., Zvolsky, P. & Walsh, M. Mode of inheritance in families of patients with lithium-responsive affective disorders. *Acta Psychiatr. Scand.* **90**, 304–310

(1994).

11. Potash, J. B. *et al.* The familial aggregation of psychotic symptoms in bipolar disorder pedigrees. *Am. J. Psychiatry* **158**, 1258–1264 (2001).
12. Jones, I. & Craddock, N. Do puerperal psychotic episodes identify a more familial subtype of bipolar disorder? Results of a family history study. *Psychiatr. Genet.* **12**, 177–180 (2002).
13. MacKinnon, D. F., McMahon, F. J., Simpson, S. G., McInnis, M. G. & DePaulo, J. R. Panic disorder with familial bipolar disorder. *Biol. Psychiatry* **42**, 90–95 (1997).
14. Angst, J., Frey, R., Lohmeyer, B. & Zerbin-Rüdin, E. Bipolar manic-depressive psychoses: results of a genetic investigation. *Hum. Genet.* **55**, 237–254 (1980).
15. Angst, J. & Grobler, C. Unipolar mania: a necessary diagnostic concept. *Eur. Arch. Psychiatry Clin. Neurosci.* **265**, 273–280 (2015).
16. Charney, A. W. *et al.* Evidence for genetic heterogeneity between clinical subtypes of bipolar disorder. *Transl. Psychiatry* **7**, e993 (2017).
17. Psychiatric GWAS Consortium Bipolar Disorder Working Group. Large-scale genome-wide association analysis of bipolar disorder identifies a new susceptibility locus near ODZ4. *Nat. Genet.* **43**, 977–983 (2011).
18. Baum, A. E. *et al.* A genome-wide association study implicates diacylglycerol kinase eta (DGKH) and several other genes in the etiology of bipolar disorder. *Mol. Psychiatry* **13**, 197–207 (2008).
19. Chen, D. T. *et al.* Genome-wide association study meta-analysis of European and Asian-ancestry samples identifies three novel loci associated with bipolar disorder. *Mol. Psychiatry* **18**, 195–205 (2013).

20. Mühleisen, T. W. *et al.* Genome-wide association study reveals two new risk loci for bipolar disorder. *Nat. Commun.* **5**, 3339 (2014).
21. Mullins, N. *et al.* Genome-wide association study of more than 40,000 bipolar disorder cases provides new insights into the underlying biology. *Nat. Genet.* **53**, 817–829 (2021).
22. Palmer, D. S. *et al.* Exome sequencing in bipolar disorder identifies AKAP11 as a risk gene shared with schizophrenia. *Nat. Genet.* **54**, 541–547 (2022).
23. Sullivan, P. IS BRAIN CELL TYPE THE KEY READOUT OF GWAS? *Eur. Neuropsychopharmacol.* **63**, e35 (2022).
24. Skene, N. G. *et al.* Genetic identification of brain cell types underlying schizophrenia. *Nat. Genet.* **50**, 825–833 (2018).
25. Bryois, J. *et al.* Genetic identification of cell types underlying brain complex traits yields insights into the etiology of Parkinson's disease. *Nat. Genet.* **52**, 482–493 (2020).
26. Cade, J. F. J. Lithium salts in the treatment of psychotic excitement. *Med. J. Aust.* **2**, 349–352 (1949).
27. Chen, P. *et al.* Mood stabilizers and risk of all-cause, natural, and suicide mortality in bipolar disorder: A nationwide cohort study. *Acta Psychiatr. Scand.* **147**, 234–247 (2023).
28. Tondo, L. *et al.* Clinical use of lithium salts: guide for users and prescribers. *Int. J. Bipolar Disord.* **7**, (2019).
29. Burdick, K. E. *et al.* The association between lithium use and neurocognitive performance in patients with bipolar disorder. *Neuropsychopharmacology* **45**, 1743–1749 (2020).

30. Hou, L. *et al.* Genetic variants associated with response to lithium treatment in bipolar disorder: a genome-wide association study. *The Lancet* **387**, 1085–1093 (2016).
31. Papiol, S., Schulze, T. G. & Alda, M. Genetics of Lithium Response in Bipolar Disorder. *Pharmacopsychiatry* **51**, 206–211 (2018).
32. Dudev, T., Mazmanian, K., Weng, W. H., Grauffel, C. & Lim, C. Free and Bound Therapeutic Lithium in Brain Signaling. *Acc. Chem. Res.* **52**, 2960–2970 (2019).
33. Hallcher, L. M. & Sherman, W. R. The effects of lithium ion and other agents on the activity of myo-inositol-1-phosphatase from bovine brain. *J. Biol. Chem.* **255**, 10896–10901 (1980).
34. Klein, P. S. & Melton, D. A. A molecular mechanism for the effect of lithium on development. *Proc. Natl. Acad. Sci. U. S. A.* **93**, 8455–8459 (1996).
35. Phiel, C. J. & Klein, P. S. Molecular targets of lithium action. *Annu. Rev. Pharmacol. Toxicol.* **41**, 789–813 (2001).
36. Berridge, M. J., Downes, C. P. & Hanley, M. R. Neural and developmental actions of lithium: A unifying hypothesis. *Cell* **59**, 411–419 (1989).
37. Sade, Y. *et al.* IP3 accumulation and/or inositol depletion: two downstream lithium's effects that may mediate its behavioral and cellular changes. *Transl. Psychiatry* **6**, e968 (2016).
38. Gould, T. D., Zarate, C. A. & Manji, H. K. Glycogen synthase kinase-3: a target for novel bipolar disorder treatments. *J. Clin. Psychiatry* **65**, 10–21 (2004).
39. Busa, W. B. & Gimlich, R. L. Lithium-induced teratogenesis in frog embryos prevented by a polyphosphoinositide cycle intermediate or a diacylglycerol analog. *Dev. Biol.* **132**, 315–324 (1989).

40. Azab, A. N., He, Q., Ju, S., Li, G. & Greenberg, M. L. Glycogen synthase kinase-3 is required for optimal de novo synthesis of inositol. *Mol. Microbiol.* **63**, 1248–1258 (2007).
41. Ye, C. & Greenberg, M. L. Inositol synthesis regulates the activation of GSK-3α in neuronal cells. *J. Neurochem.* **133**, 273–283 (2015).
42. Fan, T. W. M. *et al.* Stable isotope-resolved metabolomic analysis of lithium effects on glial-neuronal metabolism and interactions. *Metabolomics* **6**, 165–179 (2010).
43. Friede, R. L. The Enzymatic Response of Astrocytes To Various Ions in Vitro. *J. Cell Biol.* **20**, 5–15 (1964).
44. Santos, R. *et al.* Differentiation of Inflammation-Responsive Astrocytes from Glial Progenitors Generated from Human Induced Pluripotent Stem Cells. *Stem Cell Rep.* **8**, 1757–1769 (2017).
45. Vadodaria, K. C. *et al.* Altered Neuronal Support and Inflammatory Response in Bipolar Disorder Patient-Derived Astrocytes. *Stem Cell Rep.* **16**, 825–835 (2021).
46. Rivera, A. D. & Butt, A. M. Astrocytes are direct cellular targets of lithium treatment: novel roles for lysyl oxidase and peroxisome-proliferator activated receptor-γ as astroglial targets of lithium. *Transl. Psychiatry* **9**, 211 (2019).
47. Harris, J. L., Choi, I. Y. & Brooks, W. M. Probing astrocyte metabolism in vivo: Proton magnetic resonance spectroscopy in the injured and aging brain. *Front. Aging Neurosci.* **7**, 1–8 (2015).
48. Daniel, E. D., Cheng, L., Maycox, P. R. & Mudge, A. W. The common inositol-reversible effect of mood stabilizers on neurons does not involve GSK3 inhibition, myo-inositol-1-phosphate synthase or the sodium-dependent myo-inositol transporters. *Mol. Cell. Neurosci.* **32**, 27–36 (2006).

49. Heirendt, L. *et al.* Creation and analysis of biochemical constraint-based models using the COBRA Toolbox v.3.0. *Nat. Protoc.* **14**, 639–702 (2019).
50. Leucht, S., Helfer, B., Dold, M., Kissling, W. & McGrath, J. J. Lithium for schizophrenia. *Cochrane Database Syst. Rev.* **2015**, (2015).
51. Brunk, E. *et al.* Recon3D enables a three-dimensional view of gene variation in human metabolism. *Nat. Biotechnol.* **36**, 272–281 (2018).
52. Auslander, N. *et al.* An integrated computational and experimental study uncovers FUT9 as a metabolic driver of colorectal cancer. *Mol. Syst. Biol.* **13**, 956 (2017).
53. Baloni, P. *et al.* Metabolic Network Analysis Reveals Altered Bile Acid Synthesis and Metabolism in Alzheimer's Disease. *Cell Rep. Med.* **1**, 100138 (2020).
54. Dougherty, B. V. *et al.* Identifying functional metabolic shifts in heart failure with the integration of omics data and a heart-specific, genome-scale model. *Cell Rep.* **34**, 108836 (2021).
55. Styr, B. *et al.* Mitochondrial Regulation of the Hippocampal Firing Rate Set Point and Seizure Susceptibility. *Neuron* **102**, 1009-1024.e8 (2019).
56. Zhang, Y. *et al.* Purification and Characterization of Progenitor and Mature Human Astrocytes Reveals Transcriptional and Functional Differences with Mouse. *Neuron* **89**, 37–53 (2016).
57. Koskuvi, M. *et al.* Contribution of astrocytes to familial risk and clinical manifestation of schizophrenia. *Glia* **70**, 650–660 (2022).
58. Kim, D., Paggi, J. M., Park, C., Bennett, C. & Salzberg, S. L. Graph-based genome alignment and genotyping with HISAT2 and HISAT-genotype. *Nat. Biotechnol.* **37**, 907–915 (2019).
59. Li, H. *et al.* The Sequence Alignment/Map format and SAMtools. *Bioinformatics* **25**,

2078–2079 (2009).

60. Trapnell, C. *et al.* Transcript assembly and quantification by RNA-Seq reveals unannotated transcripts and isoform switching during cell differentiation. *Nat. Biotechnol.* **28**, 511–5 (2010).
61. Uhlén, M. *et al.* Tissue-based map of the human proteome. *Science* **347**, (2015).
62. Kuo, C.-C., Chiang, A. W. T., Baghdassarian, H. M. & Lewis, N. E. Dysregulation of the secretory pathway connects Alzheimer's disease genetics to aggregate formation. *Cell Syst.* **12**, 873-884.e4 (2021).
63. Zur, H., Ruppin, E. & Shlomi, T. iMAT: an integrative metabolic analysis tool. *Bioinformatics* **26**, 3140–3142 (2010).
64. Becker, S. A. & Palsson, B. O. Context-Specific Metabolic Networks Are Consistent with Experiments. *PLoS Comput. Biol.* **4**, e1000082 (2008).
65. Jerby, L., Shlomi, T. & Ruppin, E. Computational reconstruction of tissue-specific metabolic models: Application to human liver metabolism. *Mol. Syst. Biol.* **6**, 1–9 (2010).
66. Vlassis, N., Pacheco, M. P. & Sauter, T. Fast Reconstruction of Compact Context-Specific Metabolic Network Models. *PLoS Comput. Biol.* **10**, e1003424 (2014).
67. Zhao, C. *et al.* Mutant C9orf72 human iPSC-derived astrocytes cause non-cell autonomous motor neuron pathophysiology. *Glia* **68**, 1046–1064 (2020).
68. Thiele, I. *et al.* Personalized whole-body models integrate metabolism, physiology, and the gut microbiome. *Mol. Syst. Biol.* **16**, (2020).
69. Orth, J. D., Thiele, I. & Palsson, B. Ø. What is flux balance analysis?,. *Nat Biotechnol* **28**, 245–248 (2011).
70. Sahoo, S. & Thiele, I. Predicting the impact of diet and enzymopathies on human small

intestinal epithelial cells. *Hum. Mol. Genet.* **22**, 2705–2722 (2013).

71. Cheng, K. *et al.* Genome-scale metabolic modeling reveals SARS-CoV-2-induced metabolic changes and antiviral targets. *Mol. Syst. Biol.* **17**, (2021).
72. Yizhak, K., Gabay, O., Cohen, H. & Ruppin, E. Model-based identification of drug targets that revert disrupted metabolism and its application to ageing. *Nat. Commun.* **4**, 2632 (2013).
73. Benjamini, Y. & Hochberg, Y. Controlling the False Discovery Rate: A Practical and Powerful Approach to Multiple Testing. *J. R. Stat. Soc. Ser. B Methodol.* **57**, 289–300 (1995).
74. Ganesh, S. *et al.* Exome sequencing in families with severe mental illness identifies novel and rare variants in genes implicated in Mendelian neuropsychiatric syndromes. *Psychiatry Clin. Neurosci.* **73**, 11–19 (2019).
75. Ganesh, S. *et al.* Whole exome sequencing in dense families suggests genetic pleiotropy amongst Mendelian and complex neuropsychiatric syndromes. *Sci. Rep.* **12**, 21128 (2022).
76. Syama, A. *et al.* Mutation burden profile in familial Alzheimer's disease cases from India. *Neurobiol. Aging* **64**, 158.e7-158.e13 (2018).
77. Booth, H. D. E., Hirst, W. D. & Wade-Martins, R. The Role of Astrocyte Dysfunction in Parkinson's Disease Pathogenesis. *Trends Neurosci.* **40**, 358–370 (2017).
78. Opdam, S. *et al.* A Systematic Evaluation of Methods for Tailoring Genome-Scale Metabolic Models. *Cell Syst.* **4**, 318-329.e6 (2017).
79. Dai, G., Yu, H., Kruse, M., Traynor-Kaplan, A. & Hille, B. Osmoregulatory inositol transporter SMIT1 modulates electrical activity by adjusting $PI(4,5)P_2$ levels. *Proc. Natl.*

Acad. Sci. **113**, (2016).

80. Saiardi, A. & Mudge, A. W. Lithium and fluoxetine regulate the rate of phosphoinositide synthesis in neurons: a new view of their mechanisms of action in bipolar disorder. *Transl. Psychiatry* **8**, (2018).
81. Raghu, P., Joseph, A., Krishnan, H., Singh, P. & Saha, S. Phosphoinositides: Regulators of Nervous System Function in Health and Disease. *Front. Mol. Neurosci.* **12**, (2019).
82. Flam, E. & Arany, Z. Metabolite signaling in the heart. *Nat. Cardiovasc. Res.* **2**, 504–516 (2023).
83. Mocking, R. J. T., Assies, J., Ruhé, H. G. & Schene, A. H. Focus on fatty acids in the neurometabolic pathophysiology of psychiatric disorders. *J. Inherit. Metab. Dis.* **41**, 597–611 (2018).
84. Mi, Y. *et al.* Loss of fatty acid degradation by astrocytic mitochondria triggers neuroinflammation and neurodegeneration. *Nat. Metab.* **5**, 445–465 (2023).
85. Edelman, G. M. & Gally, J. A. Degeneracy and complexity in biological systems. *Proc. Natl. Acad. Sci.* **98**, 13763–13768 (2001).
86. Igarashi, M. *et al.* Brain lipid concentrations in bipolar disorder. *J. Psychiatr. Res.* **44**, 177–182 (2010).
87. Olzmann, J. A. & Carvalho, P. Dynamics and functions of lipid droplets. *Nat. Rev. Mol. Cell Biol.* **20**, 137–155 (2019).
88. Zadoorian, A., Du, X. & Yang, H. Lipid droplet biogenesis and functions in health and disease. *Nat. Rev. Endocrinol.* **19**, 443–459 (2023).
89. Smolič, T. *et al.* Astrocytes in stress accumulate lipid droplets. *Glia* **69**, 1540–1562 (2021).

90. Windham, I. A. *et al. APOE traffics to astrocyte lipid droplets and modulates triglyceride saturation and droplet size*. http://biorxiv.org/lookup/doi/10.1101/2023.04.28.538740 (2023) doi:10.1101/2023.04.28.538740.
91. Mejhert, N. *et al.* The Lipid Droplet Knowledge Portal: A resource for systematic analyses of lipid droplet biology. *Dev. Cell* **57**, 387-397.e4 (2022).
92. Nguyen Trung, M. *et al.* Stable Isotopomers of myo-Inositol Uncover a Complex MINPP1-Dependent Inositol Phosphate Network. *ACS Cent. Sci.* **8**, 1683–1694 (2022).